PHYSICAL REVIEW D **85,** 033005 (2012)

Two-loop virtual corrections to Drell-Yan production at order $\alpha_s\alpha^3$

William B. Kilgore*
Physics Department, Brookhaven National Laboratory, Upton, New York 11973, USA

Christian Sturm†
Max-Planck-Institut für Physik, (Werner-Heisenberg-Institut), Föhringer Ring 6, 80805 München, Germany
(Received 30 September 2011; published 14 February 2012)

The Drell-Yan mechanism for the production of lepton pairs is one of the most basic processes for physics studies at hadron colliders. It is therefore important to have accurate theoretical predictions. In this work we compute the two-loop virtual mixed QCD × QED corrections to Drell-Yan production. We evaluate the Feynman diagrams by decomposing the amplitudes into a set of known master integrals and their coefficients, which allows us to derive an analytical result. We also perform a detailed study of the ultraviolet and infrared structure of the two-loop amplitude and the corresponding poles in ε. Using crossing symmetry, we also determine the corresponding two-loop result for deep inelastic scattering.

DOI: 10.1103/PhysRevD.85.033005 PACS numbers: 12.38.Bx, 12.15.Lk, 13.40.Ks

I. INTRODUCTION

The Drell-Yan process is one of the most precise probes available at hadron colliders. It allows for precise measurements of the gauge boson masses [1–3], widths [4,5], and asymmetries [6] and is very sensitive to physics beyond the Standard Model like new gauge bosons [7–10]. One reason it is such a powerful probe is its very simplicity. Its experimental signature, two leptons plus anything, is quite robust against radiative emission. Theoretically, it is perhaps the simplest process to compute at hadron colliders. It was the first hadronic scattering process to be computed at next-to-next-to-leading order (NNLO) in QCD [11,12], almost 20 years ago.

In recent years, it has become clear that electroweak corrections [13–16] to Drell-Yan production are also very important. Electroweak corrections can distort the lineshape and thereby affect the measurement of the gauge boson masses. Radiative corrections can also become very large at the high energies (several hundred GeV) which will be probed at the LHC.

An important next step to refining the prediction for Drell-Yan production is the calculation of the complete mixed QCD and electroweak corrections. Currently, only the virtual corrections to the quark—gauge boson vertex are known in the literature [17]. We embark on this project by computing the simplest gauge-invariant part, the mixed QCD × QED virtual corrections. That is, we ignore all W and Z boson interactions, and consider only virtual photon and gluon exchanges. In addition, we take all fermions to be massless (except the top quark, which does not enter into this part of the calculation). For most of the calculation, there is no barrier to including a nonvanishing lepton mass. For the box contributions, however, one would need new master integrals with two massive external legs and massive internal propagators. The effects of nonvanishing masses (at least for components that do not involve box contributions) will be added at a later stage of the project. Having computed the mixed QCD × QED virtual corrections, there are many steps still required to complete the full calculation of mixed QCD and electroweak corrections. The real corrections to QCD × QED are similar in complexity to the real corrections in the NNLO QCD calculation of Drell-Yan production, except where they involve mixed initial and final state radiation. The two-loop virtual corrections involving massive gauge bosons promise to be more challenging than the current calculation as some of the double-box master integrals that will be needed are not yet known analytically. It may be that a combination of analytic and numerical techniques will have to be employed on these contributions. The real corrections to terms involving massive vector boson exchange, however, are essentially NLO QCD calculations and can be handled by methods that are now standard.

The amplitude of the Drell-Yan process is also related to electron-positron annihilation into hadrons(quarks) and to deep inelastic scattering by crossing symmetry. In the latter reaction the kinematic invariants take on different numerical values requiring different analytic continuations of the complex functions in the amplitude compared to the Drell-Yan process.

The outline of this paper is as follows. In Sec. II, we define some generalities and our notation. In Sec. III, we give an outline of the calculation and in Sec. IV we discuss the structure of the ultraviolet and infrared poles. The results are presented in Sec. V and we present our conclusions in Sec. VI. The Appendix contains supplementary information about the next-to-leading-order process, the master integrals arising in the calculation, and the result for deep inelastic scattering.

*kilgore@bnl.gov
†sturm@mpp.mpg.de

II. GENERALITIES AND NOTATION

We study the Drell-Yan process of quark (q) antiquark ($\bar{q}$) annihilation into a charged lepton (ℓ) pair

$$q(p_1) + \bar{q}(p_2) \to \ell^-(p_3) + \ell^+(p_4), \tag{1}$$

where p_1, p_2, p_3, p_4 denote the momenta of the particles, which are all considered as incoming with $p_1 + p_2 + p_3 + p_4 = 0$. In the following we will use the Mandelstam variables

$$\begin{aligned} s &= (p_1 + p_2)^2 = (p_3 + p_4)^2, \\ t &= (p_1 + p_3)^2 = (p_2 + p_4)^2, \\ u &= (p_1 + p_4)^2 = (p_2 + p_3)^2, \end{aligned} \tag{2}$$

or $s_{ij} = (p_i + p_j)^2$ to express scalar products of the external momenta.

The differential cross section is given by

$$\frac{d\sigma^V}{d\Omega} = \frac{1}{64\pi^2 s}\frac{1}{4N_c^2}\sum_{\text{spin color}} |\mathcal{M}|^2, \tag{3}$$

where the symbol N_c denotes the number of colors of SU(N_c) and $\mathcal{M}$ is the matrix element. Within this work we consider only virtual corrections to the Drell-Yan process. The perturbative expansion of the corresponding squared matrix element is given by

$$\begin{aligned} \sum_{\substack{\text{spin}\\ \text{color}}} |\mathcal{M}|^2 = N_c \mathcal{Q}_q^2 \mathcal{Q}_\ell^2 e^4 \Bigg(& A^{(0,0)} + \left(\frac{\alpha}{\pi}\right) A^{(1,0)} + \left(\frac{\alpha_s}{\pi}\right) C_F A^{(0,1)} \\ & + \left(\frac{\alpha}{\pi}\right)\left(\frac{\alpha_s}{\pi}\right) C_F A^{(1,1)} + \ldots \Bigg), \end{aligned} \tag{4}$$

where $\mathcal{Q}_q$ and $\mathcal{Q}_\ell$ are the electric charges of the initial state quarks and the final state leptons in units of the elementary charge e. The symbols α and α_s are the fine-structure constant and the strong-coupling constant, respectively; $C_F = (N_c^2 - 1)/(2N_c)$ denotes the Casimir operator of the fundamental representation of SU(N_c). The dots stand for higher-order corrections. Here and in the following we will write the expansion of any function of α and α_s as $f(\alpha, \alpha_s) = \Sigma_{m,n} (\alpha/\pi)^m (\alpha_s/\pi)^n f^{(m,n)}$. The well-known leading-order result $A^{(0,0)}$ of Eq. (4) in $d = 4 - 2\varepsilon$ space-time dimensions reads

$$A^{(0,0)} = \frac{8}{s^2}(t^2 + u^2 - s^2\varepsilon). \tag{5}$$

The one-loop QCD [18–21] and one-loop QED corrections [13] are known. For completeness we will give the bare results for $A^{(1,0)}$ as well as for $A^{(0,1)}$ in Appendix A, since they are needed for the subtraction of the ultraviolet poles through the renormalization procedure as well as for the identification of the infrared poles. Beyond leading-order, the real corrections need to be taken into account to obtain a physical cross section.

III. CALCULATION OF THE BARE PROCESS

Depending on the nature of the electromagnetic corrections, the QCD × QED corrections to Drell-Yan production can be broken up into four classes: initial state corrections, final state corrections, mixed initial and final state corrections, and vacuum polarization corrections. Sample diagrams for each of these four classes are shown in Fig. 1.

The initial state electromagnetic corrections consist of two-loop corrections to the quark-photon vertex. A sample diagram of this class of correction is shown in Fig. 1(a). All of the diagrams that appear in this portion of the calculation are topologically identical to diagrams that appear in the two-loop QCD corrections to Drell-Yan production. By simultaneously computing the two-loop QCD corrections and verifying the known result [22], we obtain a strong check on this part of the calculation. We also include the

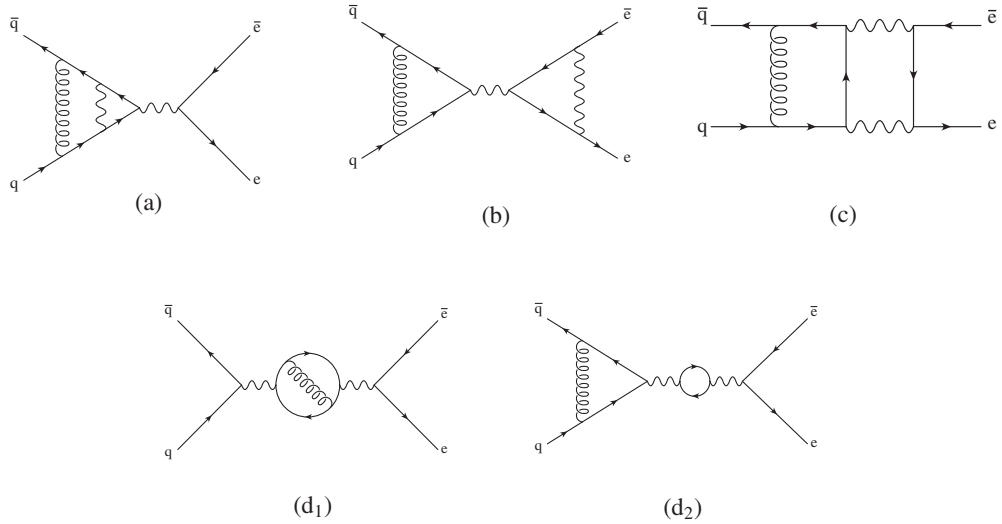

FIG. 1. Example diagrams which contribute to the two-loop mixed QCD × QED corrections. The spiral lines denote gluons, the wavy lines are photons, and the straight lines are fermions which can either be quarks in the initial state or leptons in the final state.

interference of the one-loop QCD correction and the one-loop QED initial state correction. There is but one diagram of each sort.

The final state virtual corrections are quite trivial, since the only contributing two-loop diagram is the one shown in Fig. 1(b), which is just the product of two one-loop triangle diagrams. The virtual corrections to this channel also get a contribution from the interference of the one-loop QCD corrections and the one-loop final state QED corrections. Again, there is but one diagram of each sort.

The mixed initial and final state electromagnetic corrections are the most complicated terms in this calculation and the only ones which involve the kinematic variables t and u in the loop integrals. A sample diagram is shown in Fig. 1(c). Even the interference of the one-loop amplitudes is relatively complicated as the electromagnetic part involves the sum of two one-loop box integrals.

The vacuum polarization correction terms are also easy to compute as the loops are simple two-loop propagator integrals, like that shown in Fig. 1(d_1), or the product of a one-loop propagator integral and a one-loop triangle as in Fig. 1(d_2). The interference of one-loop amplitudes is again very simple as it only involves a single vacuum polarization diagram interfered with the single one-loop QCD diagram.

We have performed two independent calculations of the virtual corrections and find complete agreement. The Feynman diagrams are generated with QGRAF [23]. The symbolic algebra program FORM [24] is used to implement the Feynman rules, to interfere the two-loop diagrams with the tree-level contribution and to reduce the result to a set of Feynman integrals to be determined. The calculation proceeds in two steps. In the first step all the loop integrals are mapped onto a small set of master integrals with the traditional integration-by-parts (IBP) method [25] in combination with Laporta's algorithm [26,27]. In the second step these master integrals are evaluated.

In one calculation, the integrals are reduced to master integrals using the program REDUZE [28]. In the second calculation, the reduction has been performed with a FORM [24,29,30] based implementation which uses the packages Q2E and EXP [31,32] to identify the different

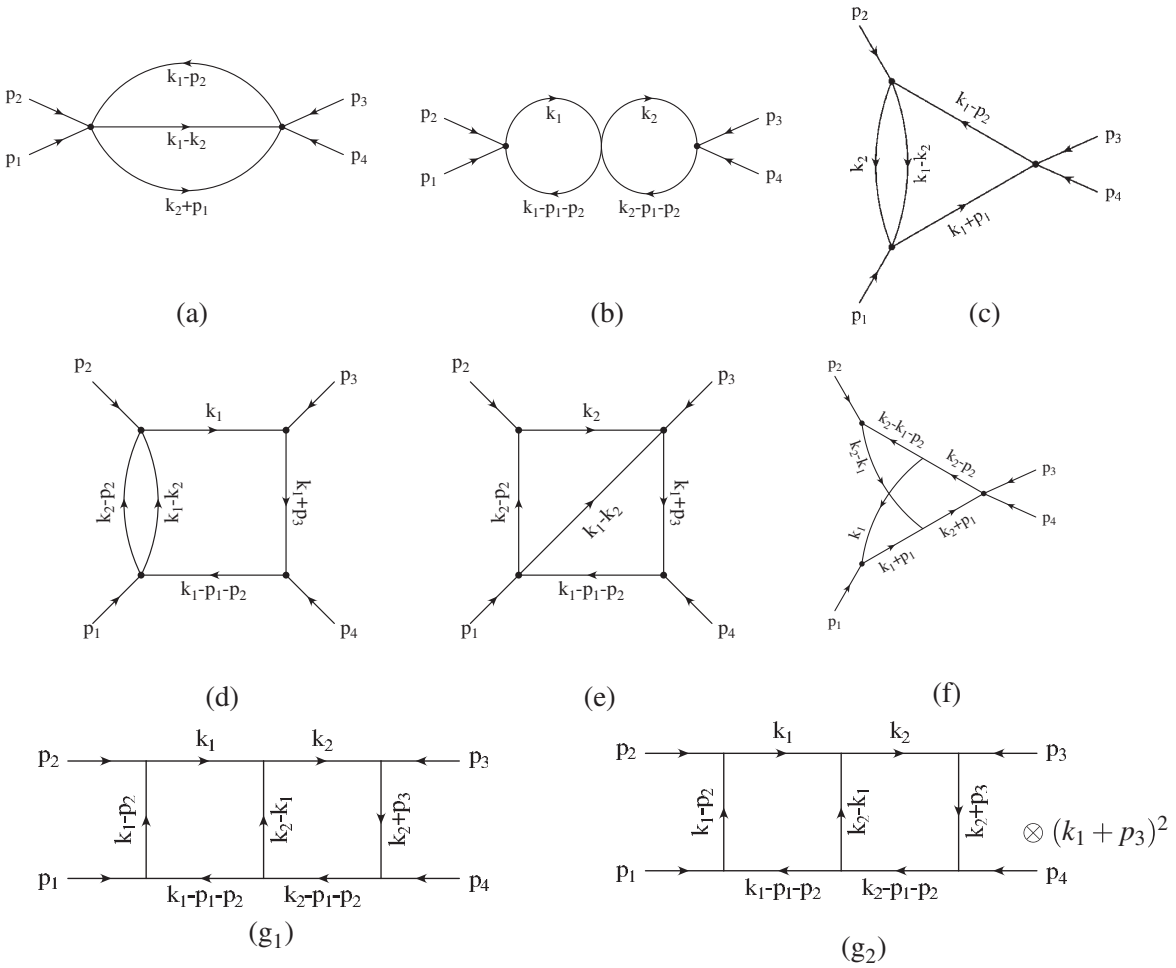

FIG. 2. The master topologies of the two-loop calculation ordered according to the number of internal lines. The arrow on the lines denotes the momentum flow. The symbols k_1 and k_2 are loop momenta. The integral representation of diagram (g_2) has an additional irreducible scalar product $(k_1 + p_3)^2$ in the numerator indicated by the ⊗ symbol.

topologies and to adopt the proper notation. The program FERMAT [33] is used to simplify the rational functions in the space-time dimension d.

We find that at the two-loop level, all integrals can be expressed in terms of eight master topologies which are shown in Fig. 2. All of the needed master integrals are known analytically in the literature to sufficiently deep order in the ε expansion and will be discussed in more detail in Appendix B. At the end, the reductions and the evaluations of the master integrals are substituted back into the FORM program to produce the final result.

IV. THE POLE STRUCTURE OF THE PROCESS

A. Ultraviolet structure and renormalization

We have performed renormalization in the $\overline{\text{MS}}$ scheme. Since we treat all particles as being massless, we only need to renormalize the couplings. Coupling constant renormalization is governed by the β-functions,

$$\beta_{\text{QED}}(\alpha,\alpha_s)=\mu^2\frac{d}{d\mu^2}\left(\frac{\alpha}{\pi}\right)=-\beta^{(2,0)}_{\text{QED}}\left(\frac{\alpha}{\pi}\right)^2-\beta^{(3,0)}_{\text{QED}}\left(\frac{\alpha}{\pi}\right)^3-\beta^{(2,1)}_{\text{QED}}\left(\frac{\alpha}{\pi}\right)^2\left(\frac{\alpha_s}{\pi}\right)+\ldots,$$
$$\beta^{(2,0)}_{\text{QED}}=-\tfrac{1}{3}(N_\ell\mathcal{Q}_\ell^2+N_cN_u\mathcal{Q}_u^2+N_cN_d\mathcal{Q}_d^2),\qquad \beta^{(3,0)}_{\text{QED}}=-\tfrac{1}{4}(N_\ell\mathcal{Q}_\ell^4+N_cN_u\mathcal{Q}_u^4+N_cN_d\mathcal{Q}_d^4),$$
$$\beta^{(2,1)}_{\text{QED}}=-\tfrac{1}{4}C_FN_c(N_u\mathcal{Q}_u^2+N_d\mathcal{Q}_d^2), \tag{6}$$

$$\beta_{\text{QCD}}(\alpha_s,\alpha)=\mu^2\frac{d}{d\mu^2}\left(\frac{\alpha_s}{\pi}\right)=-\beta^{(0,2)}_{\text{QCD}}\left(\frac{\alpha_s}{\pi}\right)^2-\beta^{(0,3)}_{\text{QCD}}\left(\frac{\alpha_s}{\pi}\right)^3-\beta^{(1,2)}_{\text{QCD}}\left(\frac{\alpha_s}{\pi}\right)^2\left(\frac{\alpha}{\pi}\right)+\ldots,\qquad \beta^{(0,2)}_{\text{QCD}}=\tfrac{11}{12}C_A-\tfrac{1}{3}T_fN_q,$$
$$\beta^{(0,3)}_{\text{QCD}}=\tfrac{17}{24}C_A^2-\tfrac{5}{12}C_AT_fN_q-\tfrac{1}{4}C_FT_fN_q,\qquad \beta^{(1,2)}_{\text{QCD}}=-\tfrac{1}{8}(N_u\mathcal{Q}_u^2+N_d\mathcal{Q}_d^2), \tag{7}$$

where μ is the renormalization scale, N_u is the number of up-type quarks, N_d is the number of down-type quarks, and N_ℓ is the number of charged leptons, while $\mathcal{Q}_u$, $\mathcal{Q}_d$, and $\mathcal{Q}_\ell$ are their electric charges, $+\frac{2}{3}$, $-\frac{1}{3}$, and -1, respectively. The symbol $C_A=N_c$ denotes the Casimir operator of the adjoint representation of SU(N_c) and $T_f=1/2$ is the normalization of the QCD charge of the fundamental representation. Note that in Eqs. (6) and (7) the superscripts i and j in the symbols $\beta^{(i,j)}_{\text{QED}}$ and $\beta^{(i,j)}_{\text{QCD}}$ represent the coefficients of α and α_s, respectively, for the $(i+j-1)$-loop β-functions of QED and QCD. This nonstandard notation emphasizes that we are expanding in two independent gauge couplings. The bare and renormalized couplings are related by

$$\left(\frac{\alpha^B}{\pi}\right)=\left(\frac{e^{\gamma_E}}{4\pi}\right)^\varepsilon\left(\frac{\alpha}{\pi}\right)\left[1-\left(\frac{\alpha}{\pi}\right)\frac{\beta^{(2,0)}}{\varepsilon}-\left(\frac{\alpha}{\pi}\right)^2\times\left(\frac{\beta^{(3,0)}}{2\varepsilon}-\left(\frac{\beta^{(2,0)}}{\varepsilon}\right)^2\right)-\left(\frac{\alpha}{\pi}\right)\left(\frac{\alpha_s}{\pi}\right)\frac{\beta^{(2,1)}}{2\varepsilon}+\ldots\right], \tag{8}$$

$$\left(\frac{\alpha_s^B}{\pi}\right)=\left(\frac{e^{\gamma_E}}{4\pi}\right)^\varepsilon\left(\frac{\alpha_s}{\pi}\right)\left[1-\left(\frac{\alpha_s}{\pi}\right)\frac{\beta^{(0,2)}}{\varepsilon}-\left(\frac{\alpha_s}{\pi}\right)^2\times\left(\frac{\beta^{(0,3)}}{2\varepsilon}-\left(\frac{\beta^{(0,2)}}{\varepsilon}\right)^2\right)-\left(\frac{\alpha}{\pi}\right)\left(\frac{\alpha_s}{\pi}\right)\frac{\beta^{(1,2)}}{2\varepsilon}+\ldots\right], \tag{9}$$

where $e\simeq 2.71828$ is Euler's number and $\gamma_E\simeq 0.577216$ is the Euler-Mascheroni constant. Since the leading-order contribution to the squared matrix element is of order α^2 and we compute terms through order $\alpha^3\alpha_s$, we need to keep QED renormalization terms proportional to $\beta^{(2,0)}$ and $\beta^{(2,1)}$ [34], while QCD renormalization does not contribute to our result. The fine-structure constant can be converted, if needed, from the above $\overline{\text{MS}}$ scheme to the on-shell definition with a conversion factor. This conversion is known to four-loop order in QED [35,36].

B. Infrared structure

An important check on our calculation is to verify that we have obtained the correct infrared structure. Some years ago, Catani [37] proposed a formula predicting the leading poles (ε^{-4} through ε^{-2}) of two-loop QCD amplitudes. At that time, the ε^{-1} poles were presumed to be process dependent and therefore unpredictable. Nonetheless, direct calculations [38–42] showed that the ε^{-1} terms seemed to follow a simple pattern based upon the numbers of quarks and gluons that made up the external legs of the amplitude.

Subsequently, Sterman and Tejeda-Yeomans [43] reformulated Catani's observation and identified the origins of the various terms. They also identified the then-unknown term, the second-order correction to the so-called "soft anomalous dimension" which prevented the prediction of the ε^{-1} terms. Aybat, Dixon, and Sterman [44,45] have since computed the two-loop corrections to the soft anomalous dimension, permitting the prediction of the full infrared structure of two-loop QCD amplitudes.

C. The infrared structure of QCD amplitudes

For a general $2\to n$ scattering process,

$$f_1(p_1,c_1)+f_2(p_2,c_2)\to f_3(p_3,c_3)+\ldots+f_{n+2}(p_{n+2},c_{n+2}), \tag{10}$$

where f_i represent the flavors of the partons, p_i their momenta, and c_i their colors, we can write the amplitude

as a vector in the space of color tensors $\{(C_I)_{\{c_i\}}\}$ as [37,46,47]

$$\left|\mathcal{M}_{\mathbf{f}}\left(p_i,\frac{\mathcal{Q}^2}{\mu^2},\alpha_s(\mu^2),\varepsilon\right)\right\rangle\equiv\sum_L\mathcal{M}_{\mathbf{f},L}\left(p_i,\frac{\mathcal{Q}^2}{\mu^2},\alpha_s(\mu^2),\varepsilon\right)\times(C_L)_{\{c_i\}},\tag{11}$$

where $\mathcal{Q}$ is an (arbitrary) overall scale and μ is the renormalization scale.

In the formulation of Refs. [43–45], a renormalized amplitude may be factorized into three functions: the jet function $\mathcal{J}_{\mathbf{f}}$, which describes the collinear dynamics of the external partons that participate in the collision; the soft function $\mathbf{S}_{\mathbf{f}}$, which describes soft exchanges between the external partons; and the hard-scattering function $|H_{\mathbf{f}}\rangle$, which describes the short-distance scattering process

$$\begin{aligned}&\left|\mathcal{M}_{\mathbf{f}}\left(p_i,\frac{\mathcal{Q}^2}{\mu^2},\alpha_s(\mu^2),\varepsilon\right)\right\rangle\\&\quad=\mathcal{J}_{\mathbf{f}}(\alpha_s(\mu^2),\varepsilon)\mathbf{S}_{\mathbf{f}}\left(p_i,\frac{\mathcal{Q}^2}{\mu^2},\alpha_s(\mu^2),\varepsilon\right)\\&\qquad\times\left|H_{\mathbf{f}}\left(p_i,\frac{\mathcal{Q}^2}{\mu^2},\alpha_s(\mu^2)\right)\right\rangle.\end{aligned}\tag{12}$$

The notation indicates that $|H_{\mathbf{f}}\rangle$ is a vector and $\mathbf{S}_{\mathbf{f}}$ is a matrix in color-space. As with any factorization, there is considerable freedom to move terms about from one function to the others. It is convenient [44,45] to define the jet and soft functions, $\mathcal{J}_{\mathbf{f}}$ and $\mathbf{S}_{\mathbf{f}}$, so that they contain all of the infrared poles but only contain infrared poles, while all infrared finite terms are absorbed into $|H_{\mathbf{f}}\rangle$.

1. The jet function

The jet function $\mathcal{J}_{\mathbf{f}}$ is found to be the product of individual jet functions $\mathcal{J}_{f_i}$ for each of the external partons,

$$\mathcal{J}_{\mathbf{f}}(\alpha_s(\mu^2),\varepsilon)=\prod_{i\in\mathbf{f}}\mathcal{J}_i(\alpha_s(\mu^2),\varepsilon).\tag{13}$$

Each individual jet function is naturally defined in terms of the Sudakov form factor [43],

$$\mathcal{J}_i(\alpha_s(\mu^2),\varepsilon)=\mathcal{J}_{\bar{i}}(\alpha_s(\mu^2),\varepsilon)\sim\left[\mathcal{M}^{[i\bar{i}\to1]}(\alpha_s(\mu^2),\varepsilon)\right]^{1/2}.\tag{14}$$

The all-orders expression for the square root of the Sudakov form factor is [48–51]

$$\begin{aligned}J_i(\alpha_s(\mu^2),\varepsilon)=\exp\Bigg\{&\frac{1}{4}\int_0^{\mu^2}\frac{d\xi^2}{\xi^2}\Bigg[\mathcal{K}_i(\alpha_s(\mu^2),\varepsilon)\\&+\mathcal{G}_i\left(-1,\bar{\alpha}_s\left(\frac{\mu^2}{\xi^2},\alpha_s(\mu^2),\varepsilon\right),\varepsilon\right)\\&+\frac{1}{2}\int_{\xi^2}^{\mu^2}\frac{d\tilde{\mu}^2}{\tilde{\mu}^2}\gamma_{Ki}\left(\bar{\alpha}_s\left(\frac{\mu^2}{\tilde{\mu}^2},\alpha_s(\mu^2),\varepsilon\right)\right)\Bigg]\Bigg\}.\end{aligned}\tag{15}$$

The functions $\mathcal{K}_i$, $\mathcal{G}_i$, and γ_{Ki} are anomalous dimensions that can be determined from fixed-order calculations of the Sudakov form factors for quarks and gluons [22,52–57]. Note that γ_{Ki} is the cusp anomalous dimension and $\mathcal{K}_i$ is determined, order by order, from γ_{Ki}. While the $\mathcal{K}_i$ are pure pole terms, the $\mathcal{G}_i$ contain terms at higher order in ε.

The jet functions $\mathcal{J}_{f_i}$ keep only the infrared poles from the logarithm of the form factor. The expansion of the jet function to second order in α_s is

$$\ln\mathcal{J}_i(\alpha_s(\mu^2),\varepsilon)=-\left(\frac{\alpha_s}{\pi}\right)\left[\frac{1}{8\varepsilon^2}\gamma_{Ki}^{(0,1)}+\frac{1}{4\varepsilon}\mathcal{G}_i^{(0,1)}(\varepsilon)\right]+\left(\frac{\alpha_s}{\pi}\right)^2\left\{\frac{\beta_{\mathrm{QCD}}^{(0,2)}}{8}\frac{1}{\varepsilon^2}\left[\frac{3}{4\varepsilon}\gamma_{Ki}^{(0,1)}+\mathcal{G}_i^{(0,1)}(\varepsilon)\right]-\frac{1}{8}\left[\frac{\gamma_{Ki}^{(0,2)}}{4\varepsilon^2}+\frac{\mathcal{G}_i^{(0,2)}(\varepsilon)}{\varepsilon}\right]\right\}+\ldots,\tag{16}$$

where

$$\begin{aligned}&\gamma_{Ki}^{(0,1)}=2C_i,\qquad\gamma_{Ki}^{(0,2)}=C_iK=C_i\left[C_A\left(\frac{67}{18}-\zeta_2\right)-\frac{10}{9}T_fN_q\right],\qquad C_q\equiv C_F,\qquad C_g\equiv C_A,\\&\mathcal{G}_q^{(0,1)}=\frac{3}{2}C_F+\frac{\varepsilon}{2}C_F(8-\zeta_2),\qquad\mathcal{G}_g^{(0,1)}=2\beta_{\mathrm{QCD}}^{(0,2)}-\frac{\varepsilon}{2}C_A\zeta_2,\\&\mathcal{G}_q^{(0,2)}=C_F^2\left(\frac{3}{16}-\frac{3}{2}\zeta_2+3\zeta_3\right)+C_FC_A\left(\frac{2545}{432}+\frac{11}{12}\zeta_2-\frac{13}{4}\zeta_3\right)-C_FT_fN_q\left(\frac{209}{108}+\frac{1}{3}\zeta_2\right),\\&\mathcal{G}_g^{(0,2)}=4\beta_{\mathrm{QCD}}^{(0,3)}+C_A^2\left(\frac{10}{27}-\frac{11}{12}\zeta_2-\frac{1}{4}\zeta_3\right)+C_AT_fN_q\left(\frac{13}{27}+\frac{1}{3}\zeta_2\right)+\frac{1}{2}C_FT_fN_q,\end{aligned}\tag{17}$$

N_q is the number of quark flavors, and $\zeta_n=\sum_{k=1}^{\infty}1/k^n$ represents the Riemann zeta-function of integer argument n. The coefficients of the β-functions are given in Eqs. (6) and (7). Even though the $\mathcal{G}_i$ have terms at higher order in ε, we only keep terms in the expansion that contribute poles to $\ln\mathcal{J}_i$.

2. The soft function

Like the jet function, the soft function can be defined in terms of eikonal amplitudes and is determined entirely by the soft anomalous dimension matrix $\mathbf{\Gamma}_{S_f}$,

$$\mathbf{S}_{\mathbf{f}}\left(p_i, \frac{\mathcal{Q}^2}{\mu^2}, \alpha_s(\mu^2), \varepsilon\right) = \mathrm{P}\exp\left\{-\frac{1}{2}\int_0^{\mu^2}\frac{d\bar{\mu}^2}{\bar{\mu}^2}\mathbf{\Gamma}_{S_f}\left(\frac{s_{ij}}{\mu^2}, \bar{\alpha}_s\left(\frac{\mu^2}{\tilde{\mu}^2}, \alpha_s(\mu^2), \varepsilon\right)\right)\right\}$$
$$= 1 + \frac{1}{2\varepsilon}\left(\frac{\alpha_s}{\pi}\right)\mathbf{\Gamma}^{(0,1)}_{S_f} + \frac{1}{8\varepsilon^2}\left(\frac{\alpha_s}{\pi}\right)^2\mathbf{\Gamma}^{(0,1)}_{S_f}\times\mathbf{\Gamma}^{(0,1)}_{S_f} - \frac{\beta^{(0,2)}_{\mathrm{QCD}}}{4\varepsilon^2}\left(\frac{\alpha_s}{\pi}\right)^2\mathbf{\Gamma}^{(0,1)}_{S_f} + \frac{1}{4\varepsilon}\left(\frac{\alpha_s}{\pi}\right)^2\mathbf{\Gamma}^{(0,2)}_{S_f}. \quad (18)$$

In the color-space notation of Refs. [37,46,47], the soft anomalous dimension is given by [44,45]

$$\mathbf{\Gamma}^{(0,1)}_{S_f} = \frac{1}{2}\sum_{i\in\mathbf{f}}\sum_{j\neq i}\mathbf{T}_i\cdot\mathbf{T}_j\ln\left(\frac{\mu^2}{-s_{ij}}\right), \quad \mathbf{\Gamma}^{(0,2)}_{S_f} = \frac{K}{2}\mathbf{\Gamma}^{(0,1)}_{S_f}, \quad (19)$$

where $K = C_A(67/18 - \zeta_2) - 10T_fN_q/9$ is the same constant that relates the one- and two-loop cusp anomalous dimensions. The $\mathbf{T}_i$ are the color generators in the representation of parton i, multiplied by ± 1, depending on whether the parton is a particle or antiparticle and whether it is incoming or outgoing. In particular, outgoing quarks and gluons and incoming antiquarks are multiplied by $+1$, while incoming quarks and gluons and outgoing antiquarks are multiplied by -1. The conservation of color-charge is enforced by the identity $\sum_i \mathbf{T}_i = 0$. Another useful identity is that $\mathbf{T}_i\cdot\mathbf{T}_i = C_i$. We note that there has been a great deal of work recently to understand the infrared structure of both massless and massive QCD amplitudes at two loops and beyond [58–63], which explains the particularly simple form of the two-loop corrections to the cusp and soft anomalous dimensions.

D. The infrared structure of QED amplitudes

It has been found that the same factorization described in Eq. (12) can be applied to pure QED amplitudes [42,64]. The two-loop amplitudes for Bhabha scattering and for $e^+e^-\to\gamma\gamma$ in massless QED were found to obey the factorization formula of Catani [37] once the proper adjustments are made to transform the QCD anomalous dimensions into QED anomalous dimensions.

The changes are as follows. The factors of the adjoint representation Casimir, C_A, originate from the gluon self-interactions. As photons have no self-interactions, C_A is set to zero. The fundamental representation Casimir, C_F is replaced by the squared electric charge of the fermion, $C_F\to\mathcal{Q}_i^2$. The factors of T_fN_q originate from inserting fermion bubbles into the gluon propagators. In QED, the different types of fermions would be weighted by the squares of their electric charges, $T_fN_q\to N_cN_u\mathcal{Q}_u^2 + N_cN_d\mathcal{Q}_d^2 + N_\ell\mathcal{Q}_\ell^2$. In the soft anomalous dimension, the color-charge matrices $\mathbf{T}_i$ are replaced by the (scalar) electric charges $\mathcal{Q}_i$. With these changes, the anomalous dimensions for the QED jet function are

$$\gamma^{(1,0)}_{Ki} = 2\mathcal{Q}_i^2, \quad \gamma^{(2,0)}_{Ki} = \mathcal{Q}_i^2K^{\mathrm{QED}} = \frac{10}{3}\mathcal{Q}_i^2\beta^{(2,0)}_{\mathrm{QED}},$$
$$\mathcal{G}^{(1,0)}_f = \frac{3}{2}\mathcal{Q}_f^2 + \frac{\varepsilon}{2}\mathcal{Q}_f^2(8-\zeta_2),$$
$$\mathcal{G}^{(2,0)}_f = \mathcal{Q}_f^4\left(\frac{3}{16} - \frac{3}{2}\zeta_2 + 3\zeta_3\right) + \mathcal{Q}_f^2\beta^{(2,0)}_{\mathrm{QED}}\left(\frac{209}{36} + \zeta_2\right), \quad (20)$$
$$\mathcal{G}^{(1,0)}_\gamma = 2\beta^{(2,0)}_{\mathrm{QED}}, \quad \mathcal{G}^{(2,0)}_\gamma = 2\beta^{(3,0)}_{\mathrm{QED}},$$

while the QED contribution to the soft anomalous dimension is

$$\mathbf{\Gamma}^{(1,0)}_{S_f} = \frac{1}{2}\sum_{i\in\mathbf{f}}\sum_{j\neq i}\mathcal{Q}_i\mathcal{Q}_j\ln\left(\frac{\mu^2}{-s_{ij}}\right),$$
$$\mathbf{\Gamma}^{(2,0)}_{S_f} = \frac{K^{\mathrm{QED}}}{2}\mathbf{\Gamma}^{(1,0)}_{S_f} = \frac{5}{3}\beta^{(2,0)}_{\mathrm{QED}}\mathbf{\Gamma}^{(1,0)}_{S_f}. \quad (21)$$

Using these parameters, one can predict the infrared structure of two-loop QED amplitudes, where the analog rules as in Eq. (19) apply for the signs. When comparing to the results of Refs. [42,64], one must account for the fact that those calculations are in the context of pure QED, involving only leptons and photons. As the universality of the ε^{-1} terms had not yet been established, the (color diagonal) $H^{(2)}$ factors for electrons and photons was quoted as

$$H^{(2)}_e = -\left(\frac{3}{8} - 3\zeta_2 + 6\zeta_3\right) + N'_f\left(-\frac{25}{54} + \frac{1}{2}\zeta_2\right),$$
$$H^{(2)}_\gamma = \frac{20}{27}N'^2_f + N'_f,$$

where $N'_f \equiv N_\ell\mathcal{Q}_\ell^2$. Transforming the results above into the notation of Ref. [37], we find that the $H^{(2)}$ terms may be more generally written as

$$H^{(2)}_f = -\mathcal{Q}_f^4\left(\frac{3}{8} - 3\zeta_2 + 6\zeta_3\right) + \mathcal{Q}_f^2\beta^{(2,0)}_{\mathrm{QED}}\left(\frac{25}{18} + \frac{3}{2}\zeta_2\right),$$
$$H^{(2)}_\gamma = \frac{20}{3}(\beta^{(2,0)}_{\mathrm{QED}})^2 - 4\beta^{(3,0)}_{\mathrm{QED}}, \quad (22)$$

where the subscript f indicates any charged fermion-lepton or quark. With these modifications, we find complete agreement with the results of Refs. [42,64].

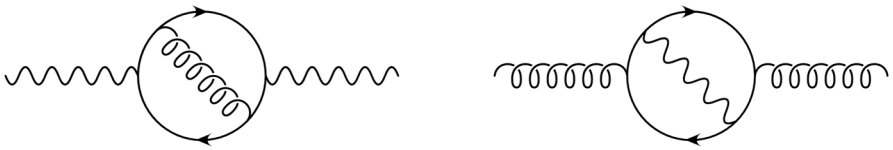

FIG. 3. Mixed second-order contributions to the QED and QCD β-functions.

E. The infrared structure of QCD × QED amplitudes

The leading terms in the infrared structure of QCD × QED corrections will come from the overlap of the one-loop terms for pure QCD and pure QED. The intrinsically QCD × QED terms will be second-order contributions to the jet and soft functions. Based upon the way the parameters were determined for QED, we can make conjectures about the parameters for QCD × QED. Since the generators for photons and gluons commute, we should again set the C_A terms to zero. We need to be a little more careful about the N_f terms, however. Our approach is to tie the N_f terms to the coefficients of the β-functions. The reason for this is that when the N_f term is part of the leading term in a β-function, it represents the insertion of a fermion bubble into a gauge boson propagator. Because the charge matrix of QCD is traceless, the bubble cannot connect a photon to a gluon and therefore these terms cannot contribute to a second-order mixed correction. When the N_f term is part of a second-order term in a β-function, however, it represents a term like those shown in Fig. 3, which can represent a second-order mixed correction. Examining the two-loop anomalous dimensions in Eqs. (17) and (19), we see that the second-order corrections to the cusp and soft anomalous dimensions are proportional to $K = C_A(67/18 - \zeta_2) - 10T_f N_q/9 = (2/3 - \zeta_2)C_A + 10/3\beta_{\rm QCD}^{(0,2)}$. Since we have argued that neither non-Abelian nor first-order β-function corrections can contribute to second-order mixed corrections, we conclude that there are no mixed corrections to the cusp and soft anomalous dimensions at this order. That leaves only the $\mathcal{G}_i$ terms. By the same reasoning as for the cusp and soft anomalous dimensions, we set the C_A and N_q terms to zero in forming $\mathcal{G}_q^{(1,1)}$, but we predict that the C_F^2 term should be transformed into $C_F\mathcal{Q}_q^2$. For $\mathcal{G}_{g,\gamma}^{(1,1)}$, we again drop the non-Abelian and first-order β-functions, but we predict that we should keep the second-order β-function terms to obtain $\mathcal{G}_g^{(1,1)} = 2\beta_{\rm QCD}^{(1,2)}$ and $\mathcal{G}_\gamma^{(1,1)} = 2\beta_{\rm QED}^{(2,1)}$.

We can thus write combined expressions for the jet and soft functions which we claim are valid through second order in both QCD and QED,

$$\begin{aligned}
&\ln\mathcal{J}_i(\alpha(\mu^2),\alpha_s(\mu^2),\varepsilon)\\
&= -\left(\frac{\alpha}{\pi}\right)\left[\frac{1}{8\varepsilon^2}\gamma_{K,i}^{(1,0)} + \frac{1}{4\varepsilon}\mathcal{G}_i^{(1,0)}(\varepsilon)\right] - \left(\frac{\alpha_s}{\pi}\right)\left[\frac{1}{8\varepsilon^2}\gamma_{K,i}^{(0,1)} + \frac{1}{4\varepsilon}\mathcal{G}_i^{(0,1)}(\varepsilon)\right] + \left(\frac{\alpha}{\pi}\right)^2\left\{\frac{\beta_{\rm QED}^{(2,0)}}{8\varepsilon^2}\left[\frac{3}{4\varepsilon}\gamma_{Ki}^{(1,0)} + \mathcal{G}_i^{(1,0)}(\varepsilon)\right]\right.\\
&\quad\left. - \frac{1}{8}\left[\frac{1}{4\varepsilon^2}\gamma_{Ki}^{(2,0)} + \frac{1}{\varepsilon}\mathcal{G}_i^{(2,0)}\right]\right\} + \left(\frac{\alpha_s}{\pi}\right)^2\left\{\frac{\beta_{\rm QCD}^{(0,2)}}{8\varepsilon^2}\left[\frac{3}{4\varepsilon}\gamma_{Ki}^{(0,1)} + \mathcal{G}_i^{(0,1)}(\varepsilon)\right] - \frac{1}{8}\left[\frac{1}{4\varepsilon^2}\gamma_{Ki}^{(0,2)} + \frac{1}{\varepsilon}\mathcal{G}_i^{(0,2)}\right]\right\} - \left(\frac{\alpha}{\pi}\right)\left(\frac{\alpha_s}{\pi}\right)\frac{1}{4\varepsilon}\mathcal{G}_i^{(1,1)} + \ldots,
\end{aligned} \tag{23}$$

and

$$\begin{aligned}
\mathbf{S_f}\left(p_i, \frac{\mathcal{Q}^2}{\mu^2}, \alpha(\mu^2), \alpha_s(\mu^2), \varepsilon\right) &= 1 + \frac{1}{2\varepsilon}\left(\frac{\alpha}{\pi}\right)\mathbf{\Gamma}_{S_f}^{(1,0)} + \frac{1}{2\varepsilon}\left(\frac{\alpha_s}{\pi}\right)\mathbf{\Gamma}_{S_f}^{(0,1)} + \frac{1}{8\varepsilon^2}\left(\frac{\alpha}{\pi}\right)^2\mathbf{\Gamma}_{S_f}^{(1,0)} \times \mathbf{\Gamma}_{S_f}^{(1,0)}\\
&\quad + \frac{1}{8\varepsilon^2}\left(\frac{\alpha_s}{\pi}\right)^2\mathbf{\Gamma}_{S_f}^{(0,1)} \times \mathbf{\Gamma}_{S_f}^{(0,1)} + \frac{1}{4\varepsilon^2}\left(\frac{\alpha}{\pi}\right)\left(\frac{\alpha_s}{\pi}\right)\mathbf{\Gamma}_{S_f}^{(1,0)} \times \mathbf{\Gamma}_{S_f}^{(0,1)} - \frac{\beta_{\rm QED}^{(1,0)}}{4\varepsilon^2}\left(\frac{\alpha}{\pi}\right)^2\mathbf{\Gamma}_{S_f}^{(1,0)}\\
&\quad - \frac{\beta_{\rm QCD}^{(0,2)}}{4\varepsilon^2}\left(\frac{\alpha_s}{\pi}\right)^2\mathbf{\Gamma}_{S_f}^{(0,1)} + \frac{1}{4\varepsilon}\left(\frac{\alpha}{\pi}\right)^2\mathbf{\Gamma}_{S_f}^{(2,0)} + \frac{1}{4\varepsilon}\left(\frac{\alpha_s}{\pi}\right)^2\mathbf{\Gamma}_{S_f}^{(0,2)},
\end{aligned} \tag{24}$$

with

$$\gamma_{Ki}^{(1,0)} = 2\mathcal{Q}_i^2, \quad \gamma_{Ki}^{(2,0)} = \gamma_{Ki}^{(1,0)} K_{QED} = \frac{10}{3}\mathcal{Q}_i^2 \beta_{\rm QED}^{(2,0)}, \quad \gamma_{Ki}^{(0,1)} = 2C_i, \quad \gamma_{Ki}^{(0,2)} = \gamma_{Ki}^{(0,1)} K_{\rm QCD} = \left[\left(\frac{2}{3} - \zeta_2\right)C_A + \frac{10}{3}\beta_{\rm QCD}^{(2,0)}\right]C_i,$$

$$\mathcal{G}_f^{(1,0)} = \frac{3}{2}\mathcal{Q}_f^2 + \frac{\varepsilon}{2}\mathcal{Q}_f^2(8-\zeta_2), \quad \mathcal{G}_f^{(2,0)} = \mathcal{Q}_f^4\left(\frac{3}{16} - \frac{3}{2}\zeta_2 + 3\zeta_3\right) + \mathcal{Q}_f^2\beta_{\rm QED}^{(2,0)}\left(\frac{209}{36} + \zeta_2\right), \quad \mathcal{G}_\gamma^{(1,0)} = 2\beta_{\rm QED}^{(2,0)}, \quad \mathcal{G}_\gamma^{(2,0)} = 2\beta_{\rm QED}^{(3,0)},$$

$$\mathcal{G}_f^{(0,1)} = \frac{3}{2}C_F + \frac{\varepsilon}{2}C_F(8-\zeta_2), \quad \mathcal{G}_f^{(0,2)} = C_F^2\left(\frac{3}{16} - \frac{3}{2}\zeta_2 + 3\zeta_3\right) + C_F C_A\left(\frac{41}{72} - \frac{13}{4}\zeta_3\right) + \beta_{\rm QCD}^{(0,2)}\left(\frac{209}{36} + \zeta_2\right),$$

$$\mathcal{G}_g^{(0,1)} = 2\beta_{\rm QCD}^{(0,2)} - \frac{\varepsilon}{2}C_A\zeta_2, \quad \mathcal{G}_g^{(0,2)} = 2\beta_{\rm QCD}^{(0,3)} + \left(\frac{19}{18} - \zeta_2\right)C_A\beta_{\rm QCD}^{(0,2)} + \left(\frac{59}{72} - \frac{1}{4}\zeta_3\right)C_A^2, \quad \mathcal{G}_f^{(1,1)} = C_F\mathcal{Q}_f^2\left(\frac{3}{16} - \frac{3}{2}\zeta_2 + 3\zeta_3\right),$$

$$\mathcal{G}_\gamma^{(1,1)} = 2\beta_{\rm QED}^{(2,1)}, \quad \mathcal{G}_g^{(1,1)} = 2\beta_{\rm QCD}^{(1,2)}, \quad \mathbf{\Gamma}_{S_f}^{(1,0)} = \frac{1}{2}\sum_{i\in\mathbf{f}}\sum_{j\neq i}\mathcal{Q}_i\mathcal{Q}_j\ln\left(\frac{\mu^2}{-s_{ij}}\right), \quad \mathbf{\Gamma}_{S_f}^{(2,0)} = \frac{K^{\rm QED}}{2}\mathbf{\Gamma}_{S_f}^{(1,0)} = \frac{5}{3}\beta_{\rm QED}^{(2,0)}\mathbf{\Gamma}_{S_f}^{(1,0)},$$

$$\mathbf{\Gamma}_{S_f}^{(0,1)} = \frac{1}{2}\sum_{i\in\mathbf{f}}\sum_{j\neq i}\mathbf{T}_i\cdot\mathbf{T}_j\ln\left(\frac{\mu^2}{-s_{ij}}\right), \quad \mathbf{\Gamma}_{S_f}^{(0,2)} = \frac{K^{\rm QCD}}{2}\mathbf{\Gamma}_{S_f}^{(0,1)} = \left[\left(\frac{1}{3} - \frac{1}{2}\zeta_2\right)C_A + \frac{5}{3}\beta_{\rm QCD}^{(2,0)}\right]\mathbf{\Gamma}_{S_f}^{(0,1)}. \tag{25}$$

F. The infrared structure of the Drell-Yan amplitude

We can now examine our result for the Drell-Yan amplitude to see if we match the expected infrared structure. We start from the factorization formula, Eq. (12), and expand both sides in powers of α and α_s,

$$|\mathcal{M}_{\rm DY}\rangle = \mathcal{J}_{\rm DY}\mathbf{S}_{\rm DY}|H_{\rm DY}\rangle \tag{26}$$

$$\begin{aligned}
&= |\mathcal{M}_{\rm DY}^{(1,0)}\rangle + \left(\frac{\alpha}{\pi}\right)|\mathcal{M}_{\rm DY}^{(2,0)}\rangle + \left(\frac{\alpha_s}{\pi}\right)|\mathcal{M}_{\rm DY}^{(1,1)}\rangle + \left(\frac{\alpha}{\pi}\right)\left(\frac{\alpha_s}{\pi}\right)|\mathcal{M}_{\rm DY}^{(2,1)}\rangle \\
&= |H_{\rm DY}^{(1,0)}\rangle + \left(\frac{\alpha}{\pi}\right)(\mathcal{J}_{\rm DY}^{(1,0)}|H_{\rm DY}^{(1,0)}\rangle + \mathbf{S}_{\rm DY}^{(1,0)}|H_{\rm DY}^{(1,0)}\rangle + |H_{\rm DY}^{(2,0)}\rangle) + \left(\frac{\alpha_s}{\pi}\right)(\mathcal{J}_{\rm DY}^{(0,1)}|H_{\rm DY}^{(1,0)}\rangle + \mathbf{S}_{\rm DY}^{(0,1)}|H_{\rm DY}^{(1,0)}\rangle + |H_{\rm DY}^{(1,1)}\rangle) + \left(\frac{\alpha}{\pi}\right)\left(\frac{\alpha_s}{\pi}\right) \\
&\quad \times[(\mathcal{J}_{\rm DY}^{(1,1)} + \mathcal{J}_{\rm DY}^{(1,0)}\mathbf{S}_{\rm DY}^{(0,1)} + \mathcal{J}_{\rm DY}^{(0,1)}\mathbf{S}_{\rm DY}^{(1,0)} + \mathbf{S}_{\rm DY}^{(1,1)})|H_{\rm DY}^{(1,0)}\rangle + (\mathcal{J}_{\rm DY}^{(1,0)} + \mathbf{S}_{\rm DY}^{(1,0)})|H_{\rm DY}^{(1,1)}\rangle + (\mathcal{J}_{\rm DY}^{(0,1)} + \mathbf{S}_{\rm DY}^{(0,1)})|H_{\rm DY}^{(2,0)}\rangle + |H_{\rm DY}^{(2,1)}\rangle].
\end{aligned} \tag{27}$$

Because of the trivial color structure of the Drell-Yan amplitude, the soft anomalous dimension matrix is proportional to the unit matrix and may be treated as a scalar function. The squared matrix element of Eq. (4) is related to the decomposition of the amplitude in Eq. (26) by

$$\sum_{\substack{\rm spin\\ \rm color}}|\mathcal{M}|^2 = (e^{\gamma_E}/(4\pi))^{2\varepsilon}\left(\frac{\alpha}{\pi}\right)^2\langle\mathcal{M}_{\rm DY}|\mathcal{M}_{\rm DY}\rangle.$$

The values of the jet and soft functions for the Drell-Yan process are given by

$$\begin{aligned}
\mathcal{J}_{\rm DY}^{(1,0)} &= -\left(\frac{1}{2\varepsilon^2} + \frac{3}{4\varepsilon}\right)(\mathcal{Q}_q^2 + \mathcal{Q}_\ell^2), \qquad \mathcal{J}_{\rm DY}^{(0,1)} = -\left(\frac{1}{2\varepsilon^2} + \frac{3}{4\varepsilon}\right)C_F, \\
\mathcal{J}_{\rm DY}^{(1,1)} &= \left(\frac{1}{4\varepsilon^4} + \frac{3}{4\varepsilon^3} + \frac{9}{16\varepsilon^2}\right)C_F(\mathcal{Q}_q^2 + \mathcal{Q}_\ell^2) - \frac{1}{2\varepsilon}\left(\frac{3}{16} - \frac{3}{2}\zeta_2 + 3\zeta_3\right)C_F\mathcal{Q}_q^2, \\
\mathbf{S}_{\rm DY}^{(1,0)} &= -\frac{1}{2\varepsilon}\left[(\mathcal{Q}_q^2 + \mathcal{Q}_\ell^2)\ln\left(\frac{\mu^2}{-s}\right) + 2\mathcal{Q}_q\mathcal{Q}_\ell\left(\ln\left(\frac{\mu^2}{-t}\right) - \ln\left(\frac{\mu^2}{-u}\right)\right)\right], \qquad \mathbf{S}_{\rm DY}^{(0,1)} = -\frac{1}{2\varepsilon}C_F\ln\left(\frac{\mu^2}{-s}\right), \\
\mathbf{S}_{\rm DY}^{(1,1)} &= \frac{1}{4\varepsilon^2}C_F\ln\left(\frac{\mu^2}{-s}\right)\left[(\mathcal{Q}_q^2 + \mathcal{Q}_\ell^2)\ln\left(\frac{\mu^2}{-s}\right) + 2\mathcal{Q}_q\mathcal{Q}_\ell\left(\ln\left(\frac{\mu^2}{-t}\right) - \ln\left(\frac{\mu^2}{-u}\right)\right)\right].
\end{aligned} \tag{28}$$

We find complete agreement between our result and the expected infrared structure presented in Eq. (28), including the intrinsically QCD $\times$ QED term in $\mathcal{J}_{\rm DY}^{(1,1)}$.

V. RESULTS

As our final result we present the interference of the finite hard-scattering terms that appear in Eq. (27), defined by

$$2\left(\frac{\alpha}{\pi}\right)^2 \mathrm{Re}[\langle H_{\mathrm{DY}}^{(1,0)}|H_{\mathrm{DY}}^{(2,1)}\rangle + \langle H_{\mathrm{DY}}^{(1,1)}|H_{\mathrm{DY}}^{(2,0)}\rangle] = N_c \mathcal{Q}_q^2 \mathcal{Q}_\ell^2 e^4 C_F B^{(1,1)}, \tag{29}$$

where we performed the renormalization in the $\overline{\mathrm{MS}}$ scheme as described in Sec. IV A. The infrared poles are subtracted in d dimensions with the help of Eqs. (27) and (28). We decompose this mixed QCD $\times$ QED two-loop contribution with respect to the charge factors

$$B^{(1,1)} = \mathcal{Q}_q \mathcal{Q}_\ell B_{q\ell}^{(1,1)} + \frac{t^2+u^2}{s^2}\left[\mathcal{Q}_q^2 B_{qq}^{(1,1)} + \mathcal{Q}_\ell^2 B_{\ell\ell}^{(1,1)} + N_c \sum_{q'} \mathcal{Q}_{q'}^2 B_{\Sigma q'}^{(1,1)} + \sum_{\ell'} \mathcal{Q}_{\ell'}^2 B_{\Sigma \ell'}^{(1,1)}\right], \tag{30}$$

where the sum over ℓ' and q' runs over all leptons and quark flavors which are active in the closed fermion loop. Each of the five terms corresponds to one of the classes of diagrams shown in FIG. 1 (a)–(d) and corresponds to a gauge-invariant subset of diagrams in this decomposition. The individual terms of Eq. (30) are

$$B_{qq}^{(1,1)} = \frac{511}{4} - \frac{83}{3}\pi^2 + \frac{67}{30}\pi^4 - 60\zeta_3 + (-93 + 10\pi^2 + 48\zeta_3)\log\left(\frac{s}{\mu^2}\right) + \left(50 - \frac{14}{3}\pi^2\right)\log^2\left(\frac{s}{\mu^2}\right) - 12\log^3\left(\frac{s}{\mu^2}\right) + 2\log^4\left(\frac{s}{\mu^2}\right), \tag{31}$$

$$B_{\ell\ell}^{(1,1)} = 128 - \frac{112}{3}\pi^2 + \frac{49}{18}\pi^4 + (14\pi^2 - 96)\log\left(\frac{s}{\mu^2}\right) + \left(50 - \frac{14}{3}\pi^2\right)\log^2\left(\frac{s}{\mu^2}\right) - 12\log^3\left(\frac{s}{\mu^2}\right) + 2\log^4\left(\frac{s}{\mu^2}\right), \tag{32}$$

$$B_{\Sigma q'}^{(1,1)} = \frac{155}{9} - \frac{140}{27}\pi^2 + 16\zeta_3 + \left(\frac{28}{9}\pi^2 - \frac{92}{3}\right)\log\left(\frac{s}{\mu^2}\right) + \frac{112}{9}\log^2\left(\frac{s}{\mu^2}\right) - \frac{8}{3}\log^3\left(\frac{s}{\mu^2}\right), \tag{33}$$

$$B_{\Sigma \ell'}^{(1,1)} = \frac{320}{9} - \frac{140}{27}\pi^2 + \left(\frac{28}{9}\pi^2 - \frac{104}{3}\right)\log\left(\frac{s}{\mu^2}\right) + \frac{112}{9}\log^2\left(\frac{s}{\mu^2}\right) - \frac{8}{3}\log^3\left(\frac{s}{\mu^2}\right), \tag{34}$$

$$\begin{aligned}
B_{q\ell}^{(1,1)} = {} & 4\frac{5u^2-t^2}{s^2}\mathrm{Li}_4\left(\frac{-u}{s}\right) - 4\left[\frac{t}{s} + 4\frac{u^2}{s^2}\log\left(\frac{-u}{s}\right)\right]\mathrm{Li}_3\left(\frac{-u}{s}\right) - \mathrm{Li}_2\left(\frac{-u}{s}\right)\left[\frac{8}{3}\frac{t^2+u^2}{s^2}\pi^2 - 2\frac{t}{s}\log\left(\frac{-u}{s}\right) - 2\frac{u}{s}\log\left(\frac{-t}{s}\right)\right. \\
& \left. - \frac{3u^2+t^2}{s^2}\log^2\left(\frac{-u}{s}\right) - \frac{3t^2+u^2}{s^2}\log^2\left(\frac{-t}{s}\right)\right] + 2\log\left(\frac{s}{\mu^2}\right)\left[2\left(\frac{7}{3}\frac{t^2+u^2}{s^2}\pi^2 - \frac{19t^2+3tu+16u^2}{s^2}\right)\log\left(\frac{-u}{s}\right)\right. \\
& \left. - 3\frac{t-u}{s}\log^2\left(\frac{-u}{s}\right)\right] + 2\log^2\left(\frac{s}{\mu^2}\right)\left[\frac{t-u}{s}\log^2\left(\frac{-u}{s}\right) + 2\frac{6u^2+tu+7t^2}{s^2}\log\left(\frac{-u}{s}\right)\right] - 8\frac{t^2+u^2}{s^2}\log^3\left(\frac{s}{\mu^2}\right)\log\left(\frac{-u}{s}\right) \\
& + 4\frac{t-u}{s}\zeta_3\left[2\log\left(\frac{-u}{s}\right) - 1\right] + \pi^2\left[\frac{4}{3}\frac{t-u}{s} + \frac{8u+15t}{3s}\log\left(\frac{-u}{s}\right) + \frac{5}{6}\frac{u^2+3t^2}{s^2}\log^2\left(\frac{-u}{s}\right)\right] - \pi^4\frac{2}{15}\frac{t-u}{s} \\
& - \frac{3u^2+t^2}{6s^2}\log^4\left(\frac{-u}{s}\right) - \frac{2}{3}\frac{t+2u}{s}\log^3\left(\frac{-u}{s}\right) - 4\frac{5u-2t}{s}\log^2\left(\frac{-u}{s}\right) - 40\frac{t}{s}\log\left(\frac{-u}{s}\right) + \frac{5t^2-u^2}{3s^2}\log^3\left(\frac{-t}{s}\right)\log\left(\frac{-u}{s}\right) \\
& - (t \leftrightarrow u),
\end{aligned} \tag{35}$$

where $\mathrm{Li}_n(z) = \sum_{k=1}^{\infty} \frac{z^k}{k^n}$ is the polylogarithm function and the symbol $(t \leftrightarrow u)$ stands for the same terms as given before only with the Mandelstam variables u and t interchanged. As an additional check of our calculation we have kept the complete dependence of the gauge parameter in the gauge boson propagators and have verified their cancellation.

VI. SUMMARY AND CONCLUSIONS

We have computed the two-loop virtual corrections to Drell-Yan production at order $\alpha_s\alpha^3$. The calculation of these mixed QCD $\times$ QED corrections includes two-loop corrections to the quark vertex, one-loop corrections to the quark and lepton vertices, vacuum polarization corrections to the photon propagator as well as two-loop box diagrams connecting the hadronic and leptonic states. The computation is accomplished by reducing all Feynman integrals to a small set of master integrals. The latter ones are known analytically to sufficiently high order in the ε expansion to allow us to derive an analytical result for the finite amplitude. In addition, we use crossing symmetry to obtain the result for the two-loop mixed QCD $\times$ QED corrections for deep inelastic scattering.

We have also shown that the infrared structure of the mixed amplitudes follows from the same universal factorization structure that governs the pure QCD and QED amplitudes and we have determined the value of the two-loop mixed anomalous dimension.

ACKNOWLEDGMENTS

We would like to thank Andreas Scharf and Doreen Wackeroth for useful discussions. This research was partially supported by the U. S. Department of Energy under Contract No. DE-AC02-98CH10886.

APPENDIX A: BARE NEXT-TO-LEADING-ORDER RESULTS IN TERMS OF MASTER INTEGRALS

We present our bare results for the next-to-leading-order processes in terms of the master integrals and coefficients to all orders in ε. For the one-loop QCD and QED corrections we adopt the decomposition of the squared matrix element as given in Eq. (4); all quantities are considered as bare. We find

$$A_B^{(0,1)} = \frac{A^{(0,0)}}{4}\left(1 - \frac{2}{\varepsilon} - 2\varepsilon\right)B_0^r(s), \tag{A1}$$

$$\begin{aligned} A_B^{(1,0)} = {} & (\mathcal{Q}_q^2 + \mathcal{Q}_\ell^2)A_B^{(0,1)} + \left(\sum_{\ell'}\mathcal{Q}_{\ell'}^2 + N_c\sum_{q'}\mathcal{Q}_{q'}^2\right)A^{(0,0)} \\ & \times\frac{1-\varepsilon}{2\varepsilon-3}B_0^r(s) + \mathcal{Q}_q\mathcal{Q}_\ell\left[\left(10 - \frac{4}{\varepsilon} - 2\varepsilon\right)\frac{t-u}{s}B_0^r(s)\right. \\ & + \left(6 - \frac{4}{\varepsilon} + 2\varepsilon\right)\frac{t-u}{s}B_0^r(u) + \left(2\frac{u(t^2+3u^2)}{s} - 3\varepsilon su\right) \\ & \left.\times D_0^r(s,u) - (t \leftrightarrow u)\right], \end{aligned} \tag{A2}$$

with the integrals

$$\begin{aligned} B_0^r(s) &= (4\pi\mu^2)^\varepsilon e^{-\varepsilon\gamma_E}2\mathrm{Re}[I_2^{(1)}(s)] \quad \text{and} \\ D_0^r(s,u) &= (4\pi\mu^2)^\varepsilon e^{-\varepsilon\gamma_E}2\mathrm{Re}[I_4^{(1)}(s,u)], \end{aligned} \tag{A3}$$

where $e \simeq 2.71828$ is again Euler's number and $\gamma_E \simeq 0.577216$ is the Euler-Mascheroni constant. The values of the master integrals $I_2^{(1)}$ and $I_4^{(1)}$ are given in Appendix B. In the coefficients of the master integrals of Eqs. (A1) and (A2), spurious poles in ε appear, which arise while solving the linear system of IBP equations. As a result, one must know the master integrals which are multiplied by such spurious poles at higher order in the ε expansion. The same situation also occurs in the two-loop amplitude. In principle, those spurious poles could be avoided by choosing an epsilon finite basis [65]. However, since all necessary master integrals are known either in closed form or to sufficiently high order in ε, we retain the standard basis of master integrals, except for the two-loop double-box topology which will be discussed in Appendix B 2.

APPENDIX B: MASTER INTEGRALS

The reduction process relates complicated integrals with many terms in the numerators and denominators to "simpler" integrals with fewer terms in both numerators and denominators. In general, it is preferred that the master integrals have numerators equal to unity, and denominators which only contain propagators of unit strength, but this preference cannot always be satisfied.

In this calculation, we encounter eighteen two-loop master integrals. Of these, eight represent distinct topologies which are shown in Fig. 2; the others are related to these eight by relabeling the external legs. Only one of the distinct topologies has an irreducible numerator (or, equivalently, a doubled propagator in the denominator).

All of the master integrals needed for this calculation are known in the literature. The double-box integrals, Fig. 2(g_1) and Fig. 2(g_2) are known as Laurent expansions in the dimensional regularization parameter ε. The others are all known in closed form and can be readily computed using standard Feynman parametrization techniques.

In the following we define the master integrals $I_{p;s}^{(k)}$ with loop momenta k_1 and k_2 in Minkowski space, where the superscript k indicates the number of loops, the subscript p denotes the number of propagators and s enumerates integrals with the same number of loops and propagators. For clarity, we also indicate the Mandelstam variables that appear as arguments.

1. One-loop master integrals

At one-loop order we have the five master integrals $I_2^{(1)}(s)$, $I_2^{(1)}(t)$, $I_2^{(1)}(u)$, $I_4^{(1)}(s,t)$, and $I_4^{(1)}(s,u)$, which are defined by

$$\begin{aligned} I_2^{(1)}(s) &= e^{\varepsilon\gamma_E}\int\frac{d^dk_1}{i\pi^{d/2}}\frac{1}{D_1D_3}, \\ I_4^{(1)}(s,u) &= e^{\varepsilon\gamma_E}\int\frac{d^dk_1}{i\pi^{d/2}}\frac{1}{D_1D_2D_3D_4}, \end{aligned} \tag{B1}$$

with

$$D_1 = k_1^2 + i\epsilon, \qquad D_2 = (k_1 - p_1)^2 + i\epsilon,$$
$$D_3 = (k_1 - p_1 - p_2)^2 + i\epsilon,$$
$$D_4 = (k_1 - p_1 - p_2 - p_3)^2 + i\epsilon.$$

Their values are

$$I_2^{(1)}(s) = e^{\varepsilon\gamma_E}(-s)^{-\varepsilon}\frac{\Gamma^2(1-\varepsilon)\Gamma(\varepsilon)}{\Gamma(2-2\varepsilon)}, \tag{B2}$$

$$I_4^{(1)}(s,t) = \frac{2e^{\varepsilon\gamma_E}}{st}\frac{\Gamma(1+\varepsilon)\Gamma^2(-\varepsilon)}{\Gamma(1-2\varepsilon)} \times\left[(-s)^{-\varepsilon}{}_2F_1\times\left(1,-\varepsilon;1-\varepsilon;1+\frac{s}{t}\right) + (-t)^{-\varepsilon}{}_2F_1\left(1,-\varepsilon;1-\varepsilon;1+\frac{t}{s}\right)\right], \tag{B3}$$

where ${}_2F_1(a,b;c;z) = \sum_{k=0}^{\infty}(a)_k(b)_k/(c)_k z^k/k!$ are hypergeometric functions, $(a)_n = \Gamma(a+n)/\Gamma(a)$ is the Pochhammer symbol, and $\Gamma(x)$ is the gamma function.

2. Two-loop master integrals

a. Three-line topologies

There is one distinct three-line topology, shown in Fig. 2(a), which we label $I_3^{(2)}(s)$ and defined by

$$I_3^{(2)}(s) = e^{2\varepsilon\gamma_E}\int\frac{d^dk_1}{i\pi^{d/2}}\frac{d^dk_2}{i\pi^{d/2}}\frac{1}{D_5D_6D_7}, \tag{B4}$$

with

$$D_5 = (k_1 - p_2)^2 + i\epsilon,$$
$$D_6 = (k_1 - k_2)^2 + i\epsilon,$$
$$D_7 = (k_2 + p_1)^2 + i\epsilon.$$

Its value is

$$I_3^{(2)}(s) = e^{2\varepsilon\gamma_E}(-s)^{1-2\varepsilon}\frac{\varepsilon^3\Gamma^3(-\varepsilon)\Gamma(-1+2\varepsilon)}{\Gamma(3-3\varepsilon)}. \tag{B5}$$

In addition, we also need $I_3^{(2)}(t)$ and $I_3^{(2)}(u)$.

b. Four-line topologies

There are four four-line master integrals, $I_{4;1}^{(2)}(s)$, $I_{4;2}^{(2)}(s)$, $I_{4;2}^{(2)}(t)$, and $I_{4;2}^{(2)}(u)$ with two distinct four-line topologies. One is a simple iterated bubble diagram, shown in Fig. 2(b), which evaluates to the square of the expression in Eq. (B2); the other is shown in Fig. 2(c). They are defined by

$$I_{4;1}^{(2)}(s) = e^{2\varepsilon\gamma_E}\int\frac{d^dk_1}{i\pi^{d/2}}\frac{d^dk_2}{i\pi^{d/2}}\frac{1}{D_1D_3D_8D_9},$$
$$I_{4;2}^{(2)}(s) = e^{2\varepsilon\gamma_E}\int\frac{d^dk_1}{i\pi^{d/2}}\frac{d^dk_2}{i\pi^{d/2}}\frac{1}{D_5D_6D_8D_{10}} \tag{B6}$$

with

$$D_8 = k_2^2 + i\epsilon,$$
$$D_9 = (k_2 - p_1 - p_2)^2 + i\epsilon,$$
$$D_{10} = (k_1 + p_1)^2 + i\epsilon,$$

and are given by $I_{4;1}^{(2)}(s) = (I_2^{(1)}(s))^2$,

$$I_{4;2}^{(2)}(s) = e^{2\varepsilon\gamma_E}(-s)^{-2\varepsilon} \times\frac{\Gamma(1-2\varepsilon)\Gamma^2(-\varepsilon)\Gamma(1+\varepsilon)\Gamma(1+2\varepsilon)}{2(1-2\varepsilon)\Gamma(2-3\varepsilon)}. \tag{B7}$$

c. Five-line topologies

There are six five-line master integrals $I_{5;1}^{(2)}(s,t,u)$, $I_{5;1}^{(2)}(u,s,t)$, $I_{5;1}^{(2)}(s,u,t)$, $I_{5;1}^{(2)}(t,s,u)$, $I_{5;2}^{(2)}(s,t,u)$, and $I_{5;2}^{(2)}(s,u,t)$ with two distinct five-line topologies, which are shown in Figs. 2(d) and 2(e). The first topology has a bubble connecting two adjacent corners of a box, the other five-line topology is a box diagram with a diagonal-line connecting opposite corners. They are defined by

$$I_{5;1}^{(2)}(s,u,t) = e^{2\varepsilon\gamma_E}\int\frac{d^dk_1}{i\pi^{d/2}}\frac{d^dk_2}{i\pi^{d/2}}\frac{1}{D_1D_3D_6D_{11}D_{12}}, \tag{B8}$$

$$I_{5;2}^{(2)}(s,u,t) = e^{2\varepsilon\gamma_E}\int\frac{d^dk_1}{i\pi^{d/2}}\frac{d^dk_2}{i\pi^{d/2}}\frac{1}{D_3D_6D_8D_{11}D_{12}}, \tag{B9}$$

with

$$D_{11} = (k_1 + p_3)^2 + i\epsilon, \qquad D_{12} = (k_2 - p_2)^2 + i\epsilon.$$

Their results read

$$I_{5;1}^{(2)}(s,u,t) = -\frac{e^{2\varepsilon\gamma_E}}{s}\frac{\Gamma^2(-\varepsilon)\Gamma(-1+2\varepsilon)}{\Gamma(1-3\varepsilon)} \times\left[(-u)^{-2\varepsilon}\Gamma(1-\varepsilon){}_2F_1\left(1,-\varepsilon;1-\varepsilon;-\frac{t}{s}\right) + (-s)^{-2\varepsilon}\Gamma(1+\varepsilon)\Gamma(1-2\varepsilon)_2 \times F_1\left(1,\varepsilon;1-\varepsilon;-\frac{t}{s}\right)\right], \tag{B10}$$

$$I_{5;2}^{(2)}(s,u,t) = e^{2\varepsilon\gamma_E}\frac{\Gamma^3(-\varepsilon)\Gamma(2\varepsilon)}{2t\Gamma(1-3\varepsilon)} \times\left[(-u)^{-2\varepsilon}\left(1-{}_2F_1\left(1,-2\varepsilon;1-2\varepsilon;-\frac{t}{s}\right)\right) + (-s)^{-2\varepsilon}\left(1-{}_2F_1\left(1,-2\varepsilon;1-2\varepsilon;-\frac{t}{u}\right)\right)\right]. \tag{B11}$$

d. Six-line topologies

There is only one six-line master integral, the nonplanar triangle diagram, shown in Fig. 2(f) and defined by

$$I_6^{(2)}(s) = e^{2\varepsilon\gamma_E}\int\frac{d^dk_1}{i\pi^{d/2}}\frac{d^dk_2}{i\pi^{d/2}}\frac{1}{D_1D_6D_7D_{10}D_{12}D_{13}},\quad \text{with}\quad D_{13}=(k_2-k_1-p_2)^2+i\epsilon.$$

Its result can be expressed with the help of generalized hypergeometric functions ${}_pF_q(a_1,\ldots,a_p;b_1,\ldots,b_q;z) = \sum_{k=0}^{\infty}(a_1)_k\ldots(a_p)_k/((b_1)_k\ldots(b_q)_k)z^k/k!$ by

$$\begin{aligned}I_6^{(2)}(s) = -e^{2\varepsilon\gamma_E}(-s)^{-2-2\varepsilon}\Gamma(1+2\varepsilon)\Bigg[&-\frac{\Gamma(1-\varepsilon)\Gamma^4(1-2\varepsilon)\Gamma(1+\varepsilon)\Gamma^2(1+2\varepsilon)}{\varepsilon^4\Gamma^2(1-4\varepsilon)\Gamma(1+4\varepsilon)}-\frac{4\Gamma^2(1-\varepsilon)\Gamma(1-2\varepsilon)}{\varepsilon^4\Gamma(1-4\varepsilon)}\\&+\frac{\Gamma^2(1-\varepsilon)\Gamma(1-2\varepsilon)\Gamma(1+\varepsilon)}{2\varepsilon^4\Gamma(1-3\varepsilon)}{}_3F_2(1,-2\varepsilon,-4\varepsilon;1-2\varepsilon,1-3\varepsilon;1)\\&+\frac{4\Gamma^2(1-\varepsilon)\Gamma(1-2\varepsilon)\Gamma(1+\varepsilon)\Gamma(1+2\varepsilon)}{\varepsilon^4\Gamma(1-4\varepsilon)\Gamma(1+3\varepsilon)}{}_3F_2(\varepsilon,\varepsilon,1+2\varepsilon;1+\varepsilon,1+3\varepsilon;1)\\&-\frac{\Gamma^3(1-\varepsilon)}{2\varepsilon^4\Gamma(1-3\varepsilon)}{}_4F_3(1,1-\varepsilon,-2\varepsilon,-4\varepsilon;1-2\varepsilon,1-2\varepsilon,1-3\varepsilon;1)\Bigg].\end{aligned}\tag{B12}$$

Note that the closed-form expression given above appears to differ slightly from that given by Ref. [66]. However, by rearranging the Γ-functions and applying various hypergeometric identities, one finds that the two expressions are exactly equal.

e. Seven-line topologies

There are four seven-line master integrals $I_{7;1}^{(2)}(s,t)$, $I_{7;1}^{(2)}(s,u)$, $I_{7;2}^{(2)}(s,t)$, and $I_{7;2}^{(2)}(s,u)$ with two distinct topologies. One is the double-box topology where all propagators are of unit strength, shown in Fig. 2(g_1). It is defined by

$$I_{7;1}^{(2)}(s,u) = e^{2\varepsilon\gamma_E}\int\frac{d^dk_1}{i\pi^{d/2}}\frac{d^dk_2}{i\pi^{d/2}}\frac{1}{D_1D_3D_5D_6D_8D_9D_{14}},\quad \text{with}\quad D_{14}=(k_2+p_3)^2+i\epsilon,\tag{B13}$$

and known as a Laurent expansion in ε [67]

$$\begin{aligned}I_{7;1}^{(2)}(s,u) = -\frac{(-s)^{-2-2\varepsilon}}{u}\Bigg\{&-\frac{4}{\varepsilon^4}+5\frac{\ell}{\varepsilon^3}-\frac{1}{\varepsilon^2}[2\ell^2-15\zeta_2]-\frac{1}{\varepsilon}\Bigg[4\mathrm{Li}_3(-x)-4\ell\mathrm{Li}_2(-x)+2\mathrm{Li}_1(-x)(\ell^2+6\zeta_2)\\&+\frac{2}{3}\ell^3+33\zeta_2\ell-\frac{65}{3}\zeta_3\Bigg]+\frac{4}{3}\ell^4+36\zeta_2\ell^2-\frac{88}{3}\zeta_3\ell+87\zeta_4-4(\mathrm{S}_{2,2}(-x)-\ell\mathrm{S}_{1,2}(-x))+44\mathrm{Li}_4(-x)\\&+4\mathrm{Li}_3(-x)(\mathrm{Li}_1(-x)-6\ell)+2\mathrm{Li}_2(-x)(\ell^2-2\ell\mathrm{Li}_1(-x)+20\zeta_2)+\mathrm{Li}_1^2(-x)(\ell^2+6\zeta_2)\\&+\frac{2}{3}\mathrm{Li}_1(-x)(4\ell^3+30\zeta_2\ell-6\zeta_3)+\mathcal{O}(\varepsilon)\Bigg\},\end{aligned}\tag{B14}$$

with $\ell=\log(x)$, $x=u/s$ and the generalized polylogarithm function $\mathrm{S}_{n,p}(z) = (-1)^{n+p-1}/(n-1)!/p!\times\int_0^1 dt'\log^{n-1}(t')\log^p(1-zt')/t'$.

There are two equivalent representations for the second seven-line topology. One is the double-box with a doubled propagator. The other representation is a double-box with an irreducible numerator, shown in Fig. 2(g_2). The latter is defined by

$$I_{7;2}^{(2)}(s,u) = e^{2\varepsilon\gamma_E}\int\frac{d^dk_1}{i\pi^{d/2}}\frac{d^dk_2}{i\pi^{d/2}}\frac{(k_1+p_3)^2}{D_1D_3D_5D_6D_8D_9D_{14}}.\tag{B15}$$

When one uses the integral with the doubled propagator, the reduction procedure generates a spurious pole in ε, meaning that one needs the double-box integrals expanded to order ε^1. When one instead uses the above double-box with an irreducible numerator, the reduction does not generate the extra pole, meaning that one only needs to expand the integrals to order ε^0.

The double-box with an irreducible numerator was first calculated in [68], with the result

$$I^{(2)}_{7;2}(s,u) = e^{2\varepsilon\gamma_E}(-s)^{-2-2\varepsilon}\Gamma^2(1+\varepsilon)\Big\{\frac{9}{4\varepsilon^4} - \frac{2}{\varepsilon^3}\ell - \frac{14\zeta_2}{\varepsilon^2} + \frac{1}{\varepsilon}\Big[\frac{4}{3}\ell^3 + 28\zeta_2\ell + 4(\ell^2+6\zeta_2)\mathrm{Li}_1(-x) + 8\mathrm{Li}_3(-x) - 8\ell\mathrm{Li}_2(-x) - 16\zeta_3\Big] - \frac{4}{3}\ell^4 - 26\zeta_2\ell^2 - \Big[\frac{16}{3}\ell^3 + 52\zeta_2\ell\Big]\mathrm{Li}_1(-x) - 5[\ell^2+6\zeta_2]\mathrm{Li}_1^2(-x) + [6\ell^2 + 20\ell\mathrm{Li}_1(-x) - 8\zeta_2]\mathrm{Li}_2(-x) + [8\ell - 20\mathrm{Li}_1(-x)]\mathrm{Li}_3(-x) + 20\mathrm{S}_{2,2}(-x) - 20\ell\mathrm{S}_{1,2}(-x) - 28\mathrm{Li}_4(-x) + [28\ell + 20\mathrm{Li}_1(-x)]\zeta_3 - 14\zeta_4 + \mathcal{O}(\varepsilon)\Big\}. \tag{B16}$$

APPENDIX C: DEEP INELASTIC SCATTERING

In Sec. V, we presented the result for the Drell-Yan process where the kinematic invariants have the property $s > 0 > t, u$. In deep inelastic scattering, $q(p_1) + \ell^-(p_4) \to q(p_2) + \ell^-(p_3)$, the kinematic invariants are in the region $u > 0 > s, t$. For this case, we present the $\overline{\mathrm{MS}}$ renormalized interference of the finite hard-scattering terms $|H_{\mathrm{DIS}}\rangle$ which are defined in complete analogy to the Drell-Yan case in Sec. IV F

$$2\Big(\frac{\alpha}{\pi}\Big)^2 \mathrm{Re}[\langle H^{(1,0)}_{\mathrm{DIS}}|H^{(2,1)}_{\mathrm{DIS}}\rangle + \langle H^{(1,1)}_{\mathrm{DIS}}|H^{(2,0)}_{\mathrm{DIS}}\rangle] = N_c\mathcal{Q}_q^2\mathcal{Q}_\ell^2 e^4 C_F C^{(1,1)}. \tag{C1}$$

For the quantity $C^{(1,1)}$, we perform the same decomposition as in Eq. (30) with

$$C^{(1,1)} = \mathcal{Q}_q\mathcal{Q}_\ell C^{(1,1)}_{q\ell} + \frac{t^2+u^2}{s^2}\Big[\mathcal{Q}_q^2 C^{(1,1)}_{qq} + \mathcal{Q}_\ell^2 C^{(1,1)}_{\ell\ell} + N_c\sum_{q'}\mathcal{Q}_{q'}^2 C^{(1,1)}_{\Sigma q'} + \sum_{\ell'}\mathcal{Q}_{\ell'}^2 C^{(1,1)}_{\Sigma\ell'}\Big]. \tag{C2}$$

The individual terms read as follows

$$C^{(1,1)}_{qq} = \frac{511}{4} + \frac{13}{3}\pi^2 - \frac{13}{30}\pi^4 - 60\zeta_3 + (-93 - 2\pi^2 + 48\zeta_3)\log\Big(\frac{-s}{\mu^2}\Big) + \Big(50 - \frac{2}{3}\pi^2\Big)\log^2\Big(\frac{-s}{\mu^2}\Big) - 12\log^3\Big(\frac{-s}{\mu^2}\Big) + 2\log^4\Big(\frac{-s}{\mu^2}\Big), \tag{C3}$$

$$C^{(1,1)}_{\ell\ell} = 128 - \frac{16}{3}\pi^2 + \frac{\pi^4}{18} + (2\pi^2 - 96)\log\Big(\frac{-s}{\mu^2}\Big) + \Big(50 - \frac{2}{3}\pi^2\Big)\log^2\Big(\frac{-s}{\mu^2}\Big) - 12\log^3\Big(\frac{-s}{\mu^2}\Big) + 2\log^4\Big(\frac{-s}{\mu^2}\Big), \tag{C4}$$

$$C^{(1,1)}_{\Sigma q'} = \frac{155}{9} - \frac{20}{27}\pi^2 + 16\zeta_3 + \Big(\frac{4}{9}\pi^2 - \frac{92}{3}\Big)\log\Big(\frac{-s}{\mu^2}\Big) + \frac{112}{9}\log^2\Big(\frac{-s}{\mu^2}\Big) - \frac{8}{3}\log^3\Big(\frac{-s}{\mu^2}\Big), \tag{C5}$$

$$C^{(1,1)}_{\Sigma\ell'} = \frac{320}{9} - \frac{20}{27}\pi^2 + \Big(\frac{4}{9}\pi^2 - \frac{104}{3}\Big)\log\Big(\frac{-s}{\mu^2}\Big) + \frac{112}{9}\log^2\Big(\frac{-s}{\mu^2}\Big) - \frac{8}{3}\log^3\Big(\frac{-s}{\mu^2}\Big), \tag{C6}$$

$$C^{(1,1)}_{q\ell} = D^{(1,1)}_{q\ell}(u,t) + E^{(1,1)}_{q\ell}(u,t), \tag{C7}$$

with

$$D_{q\ell}^{(1,1)}(u,t) = 4\frac{t^2-5u^2}{s^2}\mathrm{Li}_4\left(\frac{-s}{u}\right) - 4\left[\frac{t}{s} - 4\frac{u^2}{s^2}\log\left(\left|\frac{s}{u}\right|\right)\right]\mathrm{Li}_3\left(\frac{-s}{u}\right) + \mathrm{Li}_2\left(\frac{-s}{u}\right)\left[\frac{2}{3}\frac{t^2+u^2}{s^2}\pi^2 + 2\frac{t}{s}\log\left(\left|\frac{s}{u}\right|\right)\right.$$
$$+ 2\frac{u}{s}\log\left(\left|\frac{s}{t}\right|\right) - \frac{3u^2+t^2}{s^2}\log^2\left(\left|\frac{s}{u}\right|\right) - \frac{3t^2+u^2}{s^2}\log^2\left(\left|\frac{s}{t}\right|\right)\Big] - 2\log\left(\frac{-s}{\mu^2}\right)\Big[2\left(\frac{t^2+u^2}{3s^2}\pi^2 - \frac{19t^2+3tu+16u^2}{s^2}\right)$$
$$\times\log\left(\left|\frac{s}{u}\right|\right) + \frac{3}{2}\frac{t-u}{s}\pi^2 + 3\frac{t-u}{s}\log^2\left(\left|\frac{s}{u}\right|\right)\Big] + 2\log^2\left(\frac{-s}{\mu^2}\right)\Big[\frac{t-u}{s}\log^2\left(\left|\frac{s}{u}\right|\right)$$
$$- 2\frac{6u^2+tu+7t^2}{s^2}\log\left(\left|\frac{s}{u}\right|\right) + \frac{t-u}{s}\frac{\pi^2}{2}\Big] + 8\frac{t^2+u^2}{s^2}\log^3\left(\frac{-s}{\mu^2}\right)\log\left(\left|\frac{s}{u}\right|\right) - 4\frac{t-u}{s}\zeta_3\Big[2\log\left(\left|\frac{s}{u}\right|\right) + 1\Big]$$
$$+ \pi^2\frac{t-u}{s}\Big[\frac{25}{3} - \frac{1}{2}\log\left(\left|\frac{s}{t}\right|\right)\log\left(\left|\frac{s}{u}\right|\right)\Big] - \pi^4\frac{t-u}{5s} - \frac{3t^2+u^2}{6s^2}\log^4\left(\left|\frac{s}{u}\right|\right) + \frac{3t+4u}{3s}\log^3\left(\left|\frac{s}{u}\right|\right)$$
$$+ 4\frac{2t-5u}{s}\log^2\left(\left|\frac{s}{u}\right|\right) + 40\frac{t}{s}\log\left(\left|\frac{s}{u}\right|\right) + \frac{u}{s}\log\left(\left|\frac{s}{t}\right|\right)\log^2\left(\left|\frac{s}{u}\right|\right) + \frac{t-u}{2s}\log^2\left(\left|\frac{s}{t}\right|\right)\log^2\left(\left|\frac{s}{u}\right|\right)$$
$$+ \frac{t^2-5u^2}{3s^2}\log\left(\left|\frac{s}{t}\right|\right)\log^3\left(\left|\frac{s}{u}\right|\right) - (t\leftrightarrow u) \tag{C8}$$

and

$$E_{q\ell}^{(1,1)}(u,t) = \pi^2\Big[\frac{t-u}{s}\left(\mathrm{Li}_2\left(\frac{-s}{u}\right) - \mathrm{Li}_2\left(\frac{-s}{t}\right)\right) + \frac{t^2+19u^2}{6s^2}\log^2\left(\frac{-s}{u}\right) + \frac{5t^2-u^2}{6s^2}\log^2\left(\frac{s}{t}\right)$$
$$- 2\frac{t^2+u^2}{s^2}\log\left(\frac{s}{t}\right)\log\left(\frac{-s}{u}\right) + \frac{2}{3}\log\left(\frac{-s}{u}\right) + \frac{4}{3}\log\left(\frac{s}{t}\right) - 6\Big]. \tag{C9}$$

[1] T. Aaltonen *et al.* (CDF), Phys. Rev. Lett. **99**, 151801 (2007).
[2] T. Aaltonen *et al.* (CDF), Phys. Rev. D **77**, 112001 (2008).
[3] V. M. Abazov *et al.* (D0), Phys. Rev. Lett. **103**, 141801 (2009).
[4] T. Aaltonen *et al.* (CDF), Phys. Rev. Lett. **100**, 071801 (2008).
[5] V. M. Abazov *et al.* (D0), Phys. Rev. Lett. **103**, 231802 (2009).
[6] V. M. Abazov *et al.* (D0), Phys. Rev. Lett. **101**, 191801 (2008).
[7] V. M. Abazov *et al.* (D0), Phys. Rev. Lett. **100**, 031804 (2008).
[8] T. Aaltonen *et al.* (CDF), Phys. Rev. Lett. **102**, 031801 (2009).
[9] T. Aaltonen *et al.* (CDF), Phys. Rev. Lett. **102**, 091805 (2009).
[10] V. M. Abazov *et al.* (D0) Phys. Lett. B **695**, 88 (2011).
[11] R. Hamberg, W. L. van Neerven, and T. Matsuura, Nucl. Phys. **B359**, 343 (1991).
[12] R. V. Harlander and W. B. Kilgore, Phys. Rev. Lett. **88**, 201801 (2002).
[13] U. Baur, S. Keller, and W. K. Sakumoto, Phys. Rev. D **57**, 199 (1998).
[14] U. Baur, S. Keller, and D. Wackeroth, Phys. Rev. D **59**, 013002 (1998).
[15] U. Baur, *et al.*, Phys. Rev. D **65**, 033007 (2002).
[16] S. Dittmaier and M. Kramer, Phys. Rev. D **65**, 073007 (2002).
[17] A. Kotikov, J. H. Kühn, and O. Veretin, Nucl. Phys. **B788**, 47 (2008).
[18] J. Abad and B. Humpert, Phys. Lett. B **78**, 627 (1978).
[19] G. Altarelli, R. K. Ellis, and G. Martinelli, Nucl. Phys. **B143**, 521 (1978).
[20] J. Kubar-Andre and F. E. Paige, Phys. Rev. D **19**, 221 (1979).
[21] K. Harada, T. Kaneko, and N. Sakai, Nucl. Phys. **B155**, 169 (1979).
[22] T. Matsuura and W. L. van Neerven, Z. Phys. C **38**, 623 (1988).
[23] P. Nogueira, J. Comput. Phys. **105**, 279 (1993).
[24] J. A. M. Vermaseren, arXiv:math-ph/0010025, Report No. NIKHEF-00-0032, 2000.
[25] K. G. Chetyrkin and F. V. Tkachov, Nucl. Phys. **B192**, 159 (1981).
[26] S. Laporta and E. Remiddi, Phys. Lett. B **379**, 283 (1996).
[27] S. Laporta, Int. J. Mod. Phys. A **15**, 5087 (2000).
[28] C. Studerus, Comput. Phys. Commun. **181**, 1293 (2010).
[29] J. Vermaseren, Nucl. Phys. B, Proc. Suppl. **116**, 343 (2003).
[30] M. Tentyukov and J. Vermaseren, Comput. Phys. Commun. **176**, 385 (2007).
[31] R. Harlander, T. Seidensticker, and M. Steinhauser, Phys. Lett. B **426**, 125 (1998).
[32] T. Seidensticker, arXiv:hep-ph/9905298.

[33] R. H. Lewis, http://home.bway.net/lewis/.
[34] S. G. Gorishnii, A. L. Kataev, and S. A. Larin, Phys. Lett. B **259**, 144 (1991).
[35] D. J. Broadhurst, Z. Phys. C **54**, 599 (1992).
[36] P. Baikov, K. Chetyrkin, and C. Sturm, Nucl. Phys. B, Proc. Suppl. **183**, 8 (2008).
[37] S. Catani, Phys. Lett. B **427**, 161 (1998).
[38] C. Anastasiou, *et al.*, Nucl. Phys. **B601**, 318 (2001).
[39] C. Anastasiou, *et al.*, Nucl. Phys. **B601**, 341 (2001).
[40] C. Anastasiou, *et al.*, Phys. Lett. B **506**, 59 (2001).
[41] Z. Bern, A. De Freitas, and L. J. Dixon, J. High Energy Phys. 03 (2002) 018.
[42] C. Anastasiou, E. Glover, and M. Tejeda-Yeomans, Nucl. Phys. **B629**, 255 (2002).
[43] G. Sterman and M. E. Tejeda-Yeomans, Phys. Lett. B **552**, 48 (2003).
[44] S. Aybat, L. J. Dixon, and G. F. Sterman, Phys. Rev. Lett. **97**, 072001 (2006).
[45] S. Aybat, L. J. Dixon, and G. F. Sterman, Phys. Rev. D **74**, 074004 (2006).
[46] S. Catani and M. H. Seymour, Phys. Lett. B **378**, 287 (1996).
[47] S. Catani and M. H. Seymour, Nucl. Phys. **B485**, 291 (1997).
[48] J. C. Collins, Adv. Ser. Dir. High Energy Phys. **5**, 573 (1989).
[49] L. Magnea and G. F. Sterman, Phys. Rev. D **42**, 4222 (1990).
[50] L. Magnea, Nucl. Phys. **B593**, 269 (2001).
[51] L. Magnea, Nucl. Phys. B, Proc. Suppl. **96**, 84 (2001).
[52] R. J. Gonsalves, Phys. Rev. D **28**, 1542 (1983).
[53] G. Kramer and B. Lampe, Z. Phys. C **34**, 497 (1987).
[54] T. Matsuura, S. C. van der Marck, and W. L. van Neerven, Nucl. Phys. **B319**, 570 (1989).
[55] R. V. Harlander, Phys. Lett. B **492**, 74 (2000).
[56] S. Moch, J. Vermaseren, and A. Vogt, J. High Energy Phys. 08 (2005) 049.
[57] S. Moch, J. Vermaseren, and A. Vogt, Phys. Lett. B **625**, 245 (2005).
[58] T. Becher and M. Neubert, Phys. Rev. Lett. **102**, 162001 (2009).
[59] E. Gardi and L. Magnea, J. High Energy Phys. 03 (2009) 079.
[60] T. Becher and M. Neubert, J. High Energy Phys. 06 (2009) 081.
[61] T. Becher and M. Neubert, Phys. Rev. D **79**, 125004 (2009).
[62] E. Gardi and L. Magnea, Nuovo Cimento Soc. Ital. Fis. C **32C**, 137 (2009).
[63] L. J. Dixon, E. Gardi, and L. Magnea, J. High Energy Phys. 02 (2010) 081.
[64] Z. Bern, L. J. Dixon, and A. Ghinculov, Phys. Rev. D **63**, 053007 (2001).
[65] K. Chetyrkin, *et al.*, Nucl. Phys. **B742**, 208 (2006).
[66] T. Gehrmann, T. Huber, and D. Maitre, Phys. Lett. B **622**, 295 (2005).
[67] V. A. Smirnov, Phys. Lett. B **460**, 397 (1999).
[68] C. Anastasiou, J. B. Tausk, and M. E. Tejeda-Yeomans, Nucl. Phys. B, Proc. Suppl. **89**, 262 (2000).